SHEF-HEP/00-3,
June 2000

Measuring the SUSY Mass Scale at the LHC

D.R. Tovey *

Department of Physics and Astronomy, University of Sheffield,
Hounsfield Road, Sheffield S3 7RH, UK.

Abstract

An effective mass scale $M_{\rm susy}^{\rm eff}$ for supersymmetric particles is defined and techniques for its measurement at the LHC discussed. Monte Carlo results show that, for jets + $E_T^{\rm miss}$ events, a variable constructed from the scalar sum of the transverse momenta of all reconstructed jets together with $E_T^{\rm miss}$ provides in many cases the most accurate measurement of $M_{\rm susy}^{\rm eff}$ (intrinsic precision $\sim$ 2.1 % for mSUGRA models). The overall precision with which $M_{\rm susy}^{\rm eff}$ could be measured after given periods of LHC running and for given classes of SUSY models is calculated. The technique is extended to measurements of the total SUSY particle production cross section $\sigma_{\rm susy}$.

PACS: 12.60.Jv; 14.80.Ly; 04.65.+e
Keywords: LHC; supersymmetry; model; measurement

*e-mail: d.r.tovey@sheffield.ac.uk

1 Introduction

One of the principal motivations for construction of the Large Hadron Collider is the search for low energy supersymmetry (SUSY) [1]. In a large class of models the interactions of SUSY particles conserve R-parity, causing the Lightest Supersymmetric Particle (LSP) to be neutral and stable. R-Parity conserving SUSY events at hadron colliders are predicted to consist of cascade decays of heavy, strongly interacting SUSY particles into lighter Standard Model (SM) particles and two LSPs. This results in the classic discovery signature of an excess of events containing jets, leptons and large quantities of event missing transverse energy $E_T^{\rm miss}$ [2].

Should R-Parity conserving SUSY particles be discovered at the LHC the next task would be to measure their properties. Importantly, such measurements must be independent of the SUSY model and its parameters, which are *a priori* unknown. This process is complicated by lack of knowledge of the momenta of the two escaping LSPs in each event, preventing direct reconstruction of SUSY particle masses. Consequently other techniques are required which can measure combinations of masses indirectly. With sufficient integrated luminosity it should be possible to look for edges in the invariant mass spectra of various combinations of jets and leptons in SUSY events [2, 3], but initially the most effective technique is likely to be the use of distributions of event transverse momentum p_T and missing transverse energy [3].

The most general class of SUSY models commonly studied is the Minimal Supersymmetric Standard Model (MSSM) [1] in which the SM particle content is doubled, the Higgs sector contains two complex doublets and SUSY breaking is introduced by hand. Problematically these models also introduce many extra free parameters in addition to the 19 parameters of the SM lagrangian. In previous work [3] a very limited subset of MSSM parameter space was studied in which SUSY breaking occurs in a hidden sector of the theory and is communicated to the MSSM sector by gravitational interactions alone. These 'minimal supergravity' (mSUGRA) models [1] possess only 5 additional free parameters and are consequently more simple to work with. The reduction in the number of degrees of freedom could however artificially improve the precision with which combinations of SUSY particle masses can be measured, through the introduction of correlations between these masses. It is also not certain that if low energy SUSY is realised in nature then the one true point in parameter space lies within the mSUGRA region. An alternative region of interest is that favoured by Gauge Mediated SUSY Breaking (GMSB) models [4], in which SUSY breaking is communicated to the MSSM sector by gauge interactions. In these models the gravitino (the SUSY partner of the graviton) possesses a very small mass and forms the LSP. This is in contrast to most regions of mSUGRA and MSSM parameter space where the lightest neutralino (a superposition of the SUSY partners of the SM electroweak bosons) is often the LSP. As a result the phenomenology of GMSB models can be very different from that of these latter models.

In this letter techniques for measuring combinations of SUSY masses, similar to those used in Ref. [3] with mSUGRA models, will be investigated in detail. They will also be applied to GMSB and more general constrained MSSM models in order to assess their generality and the extent to which differing degrees of correlation between particle masses affect the measurement precision.

2 Measurement Technique

Consider a heavy SUSY particle (mass m_1) produced in a hadron-hadron collision. Assume further that this particle is boosted along the beam-axis by the longitudinal momentum imbalance of the event. If this particle undergoes a cascade decay to a lighter SUSY particle (mass m_2) and a Standard Model particle (assumed massless), then the transverse momentum p_T of the SM particle in the lab frame is related to m_1 and m_2:

$$p_T \propto \frac{1}{2}\left(m_1 - \frac{m_2^2}{m_1}\right). \quad (1)$$

Variables based on the p_T of SM particles in SUSY events are therefore sensitive to SUSY particle masses, modulo smearing effects arising from the true η distribution of those particles.

Events in the jets + $E_T^{\rm miss}$ + 0 leptons channel were used for this study. The lepton veto requirement was imposed to reduce possible systematics in the measurement arising from SM neutrino production. Defining $p_{T(i)}$ as the transverse momentum of jet i (arranged in descending order of p_T), the following four measurement variables $M_{\rm est}$ were studied:

(1) $M_{\rm est} = |p_{T(1)}| + |p_{T(2)}| + |p_{T(3)}| + |p_{T(4)}| + E_T^{\rm miss}$,

(2) $M_{\rm est} = |p_{T(1)}| + |p_{T(2)}| + |p_{T(3)}| + |p_{T(4)}|$,

(3) $M_{\rm est} = \sum_i |p_{T(i)}| + E_T^{\rm miss}$,

(4) $M_{\rm est} = \sum_i |p_{T(i)}|$.

The first variable is identical to the "effective mass" variable ($M_{\rm eff}$) defined in Ref. [3]. The scalar sum of the transverse momenta of only the four hardest jets was used due to the predominantly four-jet nature of many SUSY events [5], while the addition of the event calorimetric $E_T^{\rm miss}$ accounts for the p_T carried away by the LSPs.

Combining all jets in each detector hemisphere j into one pseudo-particle of transverse momentum $p_{T(j)}$ and invariant mass m_j, a fifth variable was also defined:

(5) $M_{\rm est} = \frac{1}{2}\sum_{j=1}^{2}\sqrt{m_j^2 + 4p_{T(j)}^2 + 2\sqrt{(m_x^2 + 2p_{T(j)}^2).(m_j^2 + 2p_{T(j)}^2)}}$.

This variable approximates the mean of the reconstructed masses of the two initial SUSY particles, assuming that each moves close to the beam axis (*i.e.*has large $|\eta|$) and decays into an LSP with (unknown) mass of order m_x. An estimated value of 100 GeV/c^2 for m_x typical of mSUGRA models was assumed in these studies. The assumed value has little effect on the final measurement precision however because $p_{T(j)}$ is in general much greater than the LSP mass.

3 Definition of Mass Scale

Due to the large number of different SUSY particles which can be produced in any given event masses measured with these variables will not correspond to those of any one particular SUSY state. Nevertheless in many models the strongly interacting SUSY particles are considerably heavier than states further down the decay chain. Hence it is the decays of these particles

which will contribute most to the sum of $|p_T|$. For this reason we shall choose to define a SUSY "mass scale" $M_{\rm susy}$ as the weighted mean of the masses of the initial SUSY particles (two per event due to R-parity conservation), with the weighting provided by the production cross section of each state:

$$M_{\rm susy} = \frac{\sum_i \sigma_i m_i}{\sum_i \sigma_i}. \tag{2}$$

This definition differs from that used in Ref. [3] but in the limit where squarks or gluinos of a single mass dominate the production cross section it gives the same result.

The above approximation breaks down for models where the lighter SUSY particles are of similar mass to the strongly interacting states. We shall attempt to compensate for this when using variables (1) - (4) by defining an effective SUSY mass scale $M_{\rm susy}^{\rm eff}$ in analogy with Eqn. (1):

$$M_{\rm susy}^{\rm eff} = \left(M_{\rm susy} - \frac{M_\chi^2}{M_{\rm susy}} \right), \tag{3}$$

where M_χ is the mass of the LSP, determined from the SUSY model. For variable (5) the equivalent expression is somewhat different:

$$M_{\rm susy}^{\rm eff} = \sqrt{M_{\rm susy}^2 - M_\chi^2}. \tag{4}$$

The effective SUSY mass scale defined by Eqn. (3) or Eqn. (4) does not correspond directly to any one SUSY particle mass or SUSY parameter. Its value for a particular SUSY model can however be determined given knowledge of the particle mass spectrum and the production cross sections in that model (using Eqn. (2)). The importance of the effective mass scale is that it is the one quantity which can be measured quickly and accurately (using the techniques described below) over large regions of SUSY parameter space. It cannot be used in isolation to determine which model has been chosen by nature but it could provide the first information capable of constraining the parameter space. The exclusion of a particular class of SUSY models may be possible using a combination of measurements of $M_{\rm susy}^{\rm eff}$ and the SUSY particle production cross section $\sigma_{\rm susy}$, as described in Sec. 6.

4 Simulation and Event Selection

Events were generated using PYTHIA 6.115 [6] (SM background, mSUGRA and constrained MSSM signal) and ISAJET 7.44 [8] (GMSB signal). The constrained MSSM class of models was that implemented in SPYTHIA, incorporating 15 free mass parameters but with no additional D-terms and with 3rd generation trilinear couplings derived from masses. For more details see Ref. [7] and references contained therein.

Hadronized events were passed through a simple simulation of a generic LHC detector. The calorimeter was assumed to have granularity $\Delta\eta \times \Delta\phi = 0.1 \times 0.1$ over the range $|\eta| < 5$, and energy resolutions $10\%/\sqrt{E} \oplus 1\%$ (ECAL), $50\%/\sqrt{E} \oplus 3\%$ (HCAL) and $100\%/\sqrt{E} \oplus 7\%$ (FCAL; $|\eta| > 3$). Jets were found with the GETJET [8] fixed cone algorithm with cone radius $\Delta R = 0.5$ and $E_T^{cut} = 50$ GeV.

Events in the jets + $E_T^{\rm miss}$ channel were selected with the following criteria:

- ≥ 4 jets with $p_T \geq 50$ GeV
- ≥ 2 jets with $p_T \geq 100$ GeV
- $E_T^{\rm miss} \geq \max(100\ {\rm GeV}, 0.25 \sum_i p_{T(i)})$
- Transverse Sphericity $S_T \geq 0.2$
- $\Delta\phi_{(\mathbf{p_{T(1)}},\mathbf{p_{T(2)}})} \leq 170^{\rm o}$
- $\Delta\phi_{(\mathbf{p_{T(1)}}+\mathbf{p_{T(2)}},\mathbf{E_T^{miss}})} \leq 90^{\rm o}$
- No muons or isolated electrons with $p_T > 10$ GeV in $|\eta| < 2.5$. A lepton identification efficiency of 90% was assumed throughout.

Standard Model background events were generated for the following processes: $t\bar{t}$ (5×10^4 events), W + jet (5×10^4 events), Z + jet (5×10^4 events) and QCD 2$\rightarrow$2 processes [6] (2.5×10^6 events). The cuts were found to pass less than 1 in 10^7 QCD events and less than 1 in 200 events from the other background channels.

The distributions of the $M_{\rm est}$ variables for background events were compared with those for SUSY signal events generated from the mSUGRA, constrained MSSM and GMSB models. In each case 100 points were randomly chosen from within the parameter space of the models, and 1×10^4 events (a factor 10 greater than in Ref. [3]) generated for each point.

For mSUGRA models the region of parameter space sampled was identical to that used in Ref. [3]: 100 GeV $< m_0 <$ 500 GeV, 100 GeV $< m_{1/2} <$ 500 GeV, -500 GeV $< A_0 <$ 500 GeV, 1.8 $< \tan(\beta) <$ 12.0 and sign(μ) = $\pm$ 1. The efficiency with which mSUGRA events passed all cuts was found to be $\sim$ 10%. For constrained MSSM models the choice of points was complicated by the requirement that models be physically realistic (positive particle masses etc.) and be suitable for this study (neutralino LSP). The masses of the strongly interacting SUSY particles and sleptons were constrained to lie in the range from 250 GeV/c^2 to 2000 GeV/c^2 while the mass parameters of the partners of the electroweak gauge bosons were constrained to lie in the range from 50 GeV/c^2 to the mass of the lightest strongly interacting SUSY particle or slepton. $\tan(\beta)$ was constrained to lie in the range $1.4 < \tan(\beta) < 100.0$. Finally, given that the lightest SUSY particles in models with low $M_{\rm susy}^{\rm eff}$ have a high probability of discovery before LHC comes on line, only those models with $M_{\rm susy}^{\rm eff} > 250$ GeV/c^2 were used. The efficiency with which constrained MSSM events passed all cuts was again found to be $\sim$ 10%.

As stated in Sec. 1, in mSUGRA and MSSM models the LSP is generally the lightest neutralino, but in GMSB models this role is taken by the gravitino. If the Next-to-Lightest Supersymmetric Particle (NLSP) is neutral and sufficiently long-lived to escape from the detector then the phenomenology is similar to that for mSUGRA or MSSM models [9]. If the NLSP is short-lived however then it decays to a gravitino and the phenomenology is different. To test whether the $M_{\rm est}$ variables defined above are also sensitive to the effective mass scales of these latter models points were chosen from within the range of GMSB parameter space defined by: 10 TeV $< \Lambda_m <$ 100 TeV, 100 TeV $< M_m <$ 1000 TeV/c^2, $1 < N_5 < 5$, 1.8 $< \tan(\beta) <$ 12.0 and sign(μ) = $\pm$ 1. The value of C_{grav}, the ratio of the gravitino mass to that expected for only one SUSY breaking scale [8], was set to unity in all cases to ensure rapid decays to the gravitino LSP. Again only those models with $M_{\rm susy}^{\rm eff} > 250$ GeV/c^2 were used. The efficiency with which GMSB events passed all cuts was found to be $\sim$ 1%.

In the mSUGRA and constrained MSSM models a statistically significant excess of signal events (S) above background (B) ($\sqrt{S+B}-\sqrt{B} \geq 5$ [10]) was found for the majority of points after the delivery of only 10 fb^{-1} of integrated luminosity (1 year of low luminosity operation). In GMSB models the data indicate that greater event statistics corresponding to at least 100 fb^{-1} (1 year of high luminosity running) would be required for discovery with these particular cuts. It should be noted however that the use of this channel and these cuts has been optimised for mSUGRA points. In GMSB models with prompt decays to gravitino LSPs photon production (bino NLSP) or lepton production (slepton NLSP) is common and consequently many events were rejected by the lepton veto and jet multiplicity requirements (hence the low signal efficiency $\sim 1\%$). In dedicated GMSB studies these requirements would likely be loosened in order to increase signal acceptance. In this case measurement variables taking account of lepton and/or photon p_T would also be used to reduce systematic measurement errors.

5 Mass Scale Measurement

The $M_{\rm est}$ distributions of SUSY signal events in the models considered here are roughly gaussian in shape (see Figs. (1) - (5) of Ref. [3]), in sharp contrast to the SM background which falls rapidly with $M_{\rm est}$. Fitting gaussian curves to the signal distributions then provides estimates of their means $\overline{M_{\rm est}}$ which can be compared with the effective mass scales $M^{\rm eff}_{\rm susy}$ of the corresponding SUSY models (Fig. 1). The 'intrinsic' or systematic precision of the measurement of $M^{\rm eff}_{\rm susy}$ can now be defined as the contribution to the scatter of the points in Fig. 1 due to different SUSY models of the same $M^{\rm eff}_{\rm susy}$ having differing $\overline{M_{\rm est}}$ values, in the limit where the $M_{\rm est}$ distributions contain infinite event statistics. The intrinsic precision is thus related to the degree of correlation between $\overline{M_{\rm est}}$ and $M^{\rm eff}_{\rm susy}$.

A typical scatter plot of $M^{\rm eff}_{\rm susy}$ against $\overline{M_{\rm est}}$ (here variable (3)) for mSUGRA models is shown in Fig. 1(a). The correlation between the variables is clearly very good. To quantify the degree of correlation a linear regression was performed on the data and the points projected onto an axis perpendicular to the fitted trendline. The distribution of the data along this line for mSUGRA models is shown in Fig. 2(a).

A scatter plot of $M^{\rm eff}_{\rm susy}$ against $\overline{M_{\rm est}}$ (again variable (3)) for constrained MSSM models is shown in Fig. 1(b). In Figs. 2(b) and (c) are plotted correlation histograms derived from this figure using the projection axis defined by the mSUGRA data. Fig. 2(b) shows the histogram obtained assuming $M^{\rm eff}_{\rm susy} = M_{\rm susy}$, while Fig. 2(c) shows the equivalent histogram using the definition of $M^{\rm eff}_{\rm susy}$ in Eqn. (3). The smaller scatter in this latter case indicates an improved measurement precision. An improvement is also obtained for mSUGRA models. Here however it is smaller since M_χ is usually much less than the masses of the strongly interacting SUSY particles [11]. In GMSB models (Fig. 1(c) and Fig. 2(d)) M_χ is negligible and so the two definitions of $M^{\rm eff}_{\rm susy}$ are always identical.

The correlation histograms were next fitted with gaussian functions. The fitted widths σ are related to the intrinsic measurement precision (defined above) but there are additional contributions due to the statistical scatter of the $\overline{M_{\rm est}}$ values arising from the use of finite Monte Carlo event statistics. These latter contributions to the fitted widths were estimated using the rms errors on the $\overline{M_{\rm est}}$ values for each histogram and then subtracted in quadrature from the fractional widths to give the intrinsic measurement precisions. Due to uncertainties

in this estimation these corrections could give unduly optimistic estimates of the measurement precisions if they were large. In all cases however the corrections were found to be small ($\lesssim$ 33%) and the effects of such uncertainties neglected. The statistical errors on the fractional widths due to finite Monte Carlo model statistics ($\sim$ 10% for mSUGRA models and $\sim$ 15% for constrained MSSM and GMSB models) were sufficiently small to justify the use of only 100 points for each parameter space scan.

Intrinsic measurement precisions for $M_{\rm susy}^{\rm eff}$ calculated using the above technique for mSUGRA, constrained MSSM and GMSB models and the five $M_{\rm est}$ variables listed in Sec. 2 are presented in Table 1. Variables (3) and (5) provide the greatest precision for mSUGRA models ($\sim$ 2.1%) while variables (3) and (4) provide the greatest precision for constrained MSSM models ($\sim$ 12.8%). The poorer precision for constrained MSSM models is apparently due to the greater number of degrees of freedom and hence the smaller correlation between the particle masses. In the GMSB models variable (4) provides the greatest measurement precision (6.1$\pm$1.0%), however variable (3) is reasonably accurate (9.0$\pm$1.2%). This indicates that effective mass scale measurements are also effective for models with gravitino LSPs.

It should be noted that for any given $M_{\rm est}$ variable the fitted means of the projected histograms (Table 1) for mSUGRA, constrained MSSM and GMSB models are consistent to within the fitted widths. For this reason it can be said that for the (admittedly limited) range of models considered here the variables provide *model independent* measurements of the effective SUSY mass scale $M_{\rm susy}^{\rm eff}$. The expected measurement precision is SUSY model dependent (due to larger widths for MSSM histograms than for mSUGRA and GMSB histograms) but this is less troublesome when comparing measurements with theory because in this case a particular SUSY model must be assumed. Further work is needed to assess whether model independence of the mass scale measurement is maintained when considering other less constrained MSSM models or even non-minimal SUSY models.

With the intrinsic precision from Table 1 for $M_{\rm est}$ variable (3) it is possible to estimate the overall precision for measuring effective SUSY mass scales in mSUGRA, constrained MSSM and GMSB models as a function of the mass scale and integrated luminosity. This overall precision contains two main contributions: that due to the intrinsic precision (which quantifies how accurately $\overline{M_{\rm est}}$ measures $M_{\rm susy}^{\rm eff}$) and that due to statistical and detector effects (which quantifies how accurately the detector measures $\overline{M_{\rm est}}$). An additional contribution comes from the statistical error on the fitted mean of the correlation histograms due to finite Monte Carlo model statistics. This manifests itself as a systematic error when performing the conversion from a measured $\overline{M_{\rm est}}$ value to an $M_{\rm susy}^{\rm eff}$ value however this is negligible when compared with the intrinsic precision, which was found to be at least an order of magnitude greater in all the cases considered here.

To estimate the overall precision distributions of $M_{\rm est}$ for signal + background events were first constructed assuming integrated luminosities of 10 fb^{-1} (1 year low luminosity), 100 fb^{-1} (1 year high lumi.) and 1000 fb^{-1} (10 years high lumi.). The mean background distribution was then subtracted from each. It is unlikely that the true distribution of background (especially QCD) events will be known with any certainty from theory or simulation. Instead the distribution of low $E_T^{\rm miss}$ events will likely be measured and the results extrapolated into the high $E_T^{\rm miss}$ region (an approach used by the CDF and D0 collaborations [12, 13]). Consequently a conservative 50% systematic error on the SM distribution was assumed when performing the background subtraction.

The signal distributions and errors (now reflecting both the statistical errors and the

systematics from the background subtraction) were again fitted with gaussian functions. The errors on the fitted means were then added in quadrature to the intrinsic precision calculated above and an estimate of the additional systematic error arising from imperfect calibration of the detector. $M_{\rm est}$ variable (3) contains contributions from both jet p_T and calorimetric $E_T^{\rm miss}$ and so systematics in the absolute measurement of both these quantities must be considered. Systematic errors associated with calibration of the jet p_T and detector $E_T^{\rm miss}$ scales of a typical LHC detector are estimated to be of order 1% and 4% respectively (data from the ATLAS collaboration [14]). The true systematic variance for each signal event is given by the weighted mean square of these quantities, with the jet p_T error dominating due to the comparatively small contribution of $E_T^{\rm miss}$ to $M_{\rm est}$. The mean of this true systematic error for each mSUGRA, constrained MSSM and GMSB model was calculated and found to be $\lesssim 1.35\%$. Consequently this conservative value was assumed for all models.

The results of this analysis are plotted in Fig. 3 for mSUGRA, constrained MSSM and GMSB models. In the last case results for 100 fb^{-1} and 1000 fb^{-1} only are presented due to the poor statistical significance of GMSB models in the jets + $E_T^{\rm miss}$ channel at low integrated luminosity. Precisions $\lesssim 15$ % (40 %) should be achievable in mSUGRA (constrained MSSM) models after only one year of low luminosity running, improving to $\lesssim 7$ % (20 %) after one year of high luminosity running. Due to the poor statistics obtainable from GMSB models, particularly for high $M_{\rm susy}^{\rm eff}$ values, measurement precisions $\lesssim 50$ % are likely to be obtainable with these cuts only after the delivery of 1000 fb^{-1} of integrated luminosity and for $M_{\rm susy}^{\rm eff}$ $\lesssim$ 1000 GeV/c^2. In all cases expected precisions are limited primarily by the process of subtracting the imperfectly known SM background at low statistics and not by systematic calibration errors.

6 Cross Section Measurement

The above technique can also be used to measure the total SUSY production cross section $\sigma_{\rm susy}$, although in this case it is the fitted normalisation of the signal $M_{\rm est}$ distribution which is of interest. The correlation between this normalisation and $\sigma_{\rm susy}$ for $M_{\rm est}$ variable (3) is shown in Fig. 4. The correlation is reasonably good with the data best fitted by a power-law. For these measurements the errors are non-gaussian (due to the power-law relation between the normalisation and $\sigma_{\rm susy}$) and in reality it is the logarithm of the measured cross section which is approximately gaussian distributed. For this reason the intrinsic measurement precisions for $\ln(\sigma_{\rm susy})$ are listed in Table 2. The overall (non-gaussian) precisions for $\sigma_{\rm susy}$ (*i.e.*$\mathrm{d}\sigma_{\rm susy}/\sigma_{\rm susy}$ = $\mathrm{d}(\ln(\sigma_{\rm susy}))$) are plotted in Fig. 5 in the same format as Fig. 3. Note that in this case in addition to the non-gaussian precision plotted in the figure an additional 5 - 10 % gaussian systematic error arising from measurement of the integrated luminosity [14] should be taken into account. This additional contribution is however small when compared with the non-gaussian error. For mSUGRA models the overall non-gaussian $\sigma_{\rm susy}$ measurement precision obtainable for 1000 fb^{-1} is $\lesssim 15$ %, while for constrained MSSM models it is $\lesssim 50$ %.

Measurements of $\sigma_{\rm susy}$ carried out in this way are inherently sensitive to the class of SUSY model, in contrast to the measurements of $M_{\rm susy}^{\rm eff}$. This is because in some models (*e.g.*GMSB) the SUSY particle decay characteristics can be such that the probability for signal events to pass the selection cuts is reduced significantly relative to that for mSUGRA models. The analysis presented here is intended to be model independent and so projects data onto a single

axis perpendicular to the trendline of the mSUGRA models. Consequently in the GMSB case, where the trend is very different from that for mSUGRA, the presented measurement precision is poor ($\gtrsim$ 300 %). If it were known that GMSB models were correct then an axis perpendicular to the GMSB trendline could be used to obtain much greater measurement precision ($\ln(\sigma_{\rm susy})$ precision $<$ 2.5 %). This highlights the fact that in reality measurements of $\sigma_{\rm susy}$, unlike measurements of $M^{\rm eff}_{\rm susy}$, are dependent on the assumed SUSY model.

It is interesting to note that by combining measurements of $M^{\rm eff}_{\rm susy}$ and $\sigma_{\rm susy}$ it may be possible to constrain certain classes of SUSY models. Consider an experimentally allowed region in $M^{\rm eff}_{\rm susy}$ - $\sigma_{\rm susy}$ parameter space defined by the measurements described above (and assuming a particular class of SUSY model for the $\sigma_{\rm susy}$ measurements). mSUGRA and GMSB models lie on sharply defined loci within this parameter space given approximately by $\sigma_{\rm susy} = 10^{-5}\exp(-0.01 M^{\rm eff}_{\rm susy})$ and $\sigma_{\rm susy} = 2\times10^{-6}\exp(-0.0075 M^{\rm eff}_{\rm susy})$ respectively, where $\sigma_{\rm susy}$ is measured in mb and $M^{\rm eff}_{\rm susy}$ is measured in GeV/c^2. Constrained MSSM models by contrast are scattered more uniformly across this parameter space. If the experimentally allowed region obtained under the assumption of a certain class of models does not coincide with the theoretically predicted locus for those models then there is clearly strong evidence for excluding them.

7 Conclusions

Techniques for measuring the effective mass scale of SUSY particles at the LHC have been investigated. Overall measurement precisions better than 15 % (40 %) should be possible for mSUGRA (constrained MSSM) models after only one year of running at low luminosity. Measurements should also be possible for models with rapid decays to gravitino LSPs, although with the requirement of either significantly increased statistics or measurement variables using photon or lepton p_T. The total SUSY production cross section should be measureable in a similar way ultimately to $\sim$ 15 % (50 %) in mSUGRA (constrained MSSM) models, although only in a model dependent manner.

Acknowledgments

The author wishes to thank Frank Paige and Craig Buttar for their careful reading of this manuscript and many helpful comments and suggestions. He also wishes to acknowledge PPARC for support under the Post-Doctoral Fellowship program.

References

[1] H.P. Nilles, *Phys. Rep.* **111** (1984) 1; H.E. Haber, G.L. Kane, *Phys. Rep.* **117** (1985) 75.

[2] H. Baer, C.-H. Chen, F. Paige, X. Tata, *Phys. Rev.* **D52** (1995) 2746; *Phys. Rev.* **D53** (1996) 6241.

[3] I. Hinchliffe, F.E. Paige, M.D. Shapiro, J. Söderqvist, W. Yao, *Phys. Rev.* **D55** (1997) 5520 9.

[4] M. Dine, W. Fischler, M. Srednicki, *Nucl. Phys.* **B189** (1981) 575.

[5] F.E. Paige, hep-ph/9801254.

[6] T. Sjöstrand, *Comput. Phys. Commun.* **82** (1994) 74.

[7] S. Mrenna, *Comput. Phys. Commun.* **101** (1997) 232.

[8] F. Paige, S. Protopopescu, in *Supercollider Physics*, ed. D. Soper (World Scientific, 1986); H. Baer, F. Paige, S. Protopopescu, X. Tata, in *Proc. Workshop on Physics at Current Accelerators and Supercolliders*, ed. J. Hewett, A. White, D. Zeppenfeld (Argonne National Laboratory, 1993).

[9] I. Hinchliffe, F.E. Paige, *Phys. Rev.* **D60** (1999) 9 095002/1.

[10] S.I. Bityukov, N.V. Krasnikov, *hep-ph/9908492.*

[11] M. Drees, S.P. Martin, in *Electroweak Symmetry Breaking and Beyond the Standard Model*, ed. T. Barklow, S. Dawson, H. Haber, S Siegrist (World Scientific, 1995) 146.

[12] F. Abe *et al.*, *Phys. Rev. Lett.* **76** (1996) 2006.

[13] B. Abbott *et al.*, *Phys. Rev. Lett.* **83** (1999) 4937 24.

[14] ATLAS Collaboration, *Detector and Physics Performance Technical Design Report*, CERN/LHCC/99-15.

Tables

Table 1: Estimates of the intrinsic $M^{\rm eff}_{\rm susy}$ measurement precision for mSUGRA, constrained MSSM and GMSB models for the five $M_{\rm est}$ variables discussed in the text. The third and fourth columns show the fitted mean and width of the projected $M^{\rm eff}_{\rm susy}$ - $\overline{M_{\rm est}}$ correlation histogram for each model and variable, and the fifth column their ratio. The sixth column shows the expected fractional width estimated from the rms error on the fitted means of the signal distributions. The seventh column contains the intrinsic measurement precision estimated by subtracting in quadrature column six from column five. Also presented in column seven are statistical errors on the intrinsic precision arising from finite Monte Carlo statistics.

Table 2: Estimates of the intrinsic $\ln(\sigma_{\rm susy})$ measurement precision for mSUGRA, constrained MSSM and GMSB models for $M_{\rm est}$ variable (3) (defined in the text). The third and fourth columns show the fitted mean and width of the projected $\ln(\sigma_{\rm susy})$ - ln(normalisation) correlation histogram for each model and variable, and the fifth column their ratio. The sixth column shows the expected fractional width estimated from the rms error on the fitted normalisations of the signal distributions. The seventh column contains the intrinsic measurement precision estimated by subtracting in quadrature column six from column five. Also presented in column seven are statistical errors on the intrinsic $\ln(\sigma_{\rm susy})$ precision arising from finite Monte Carlo statistics.

Figures

Figure 1: The effective SUSY mass scale $M_{\rm susy}^{\rm eff}$ plotted against $\overline{M_{\rm est}}$ for variable (3) (defined in the text) for 100 random mSUGRA (Fig. 1(a)), constrained MSSM (Fig. 1(b)) and GMSB (Fig. 1(c)) models. Note the differing scale in Fig. 1(c) due to the larger spread in $\overline{M_{\rm est}}$ values generated for GMSB models. In Fig. 1(c) those GMSB models where the gaussian fit to the signal $\overline{M_{\rm est}}$ distribution failed due to insufficient acceptance are omitted.

Figure 2: Projections of the points in Fig. 1 onto an axis transverse to the fitted trendline of mSUGRA data (Fig. 1(a)) for $M_{\rm est}$ variable (3). Fig. 2(a) shows the distribution for mSUGRA points, Fig. 2(b) the distribution for constrained MSSM points with $M_{\rm susy}^{\rm eff} = M_{\rm susy}$, Fig. 2(c) the distribution for constrained MSSM points with $M_{\rm susy}^{\rm eff}$ given by Eqn. (3) and Fig. 2(d) the distribution for GMSB points. Bin widths are equal in Fig. 2(b) and Fig. 2(c) to aid comparison. Bin widths differ between other plots.

Figure 3: Overall precision for measurement of $M_{\rm susy}^{\rm eff}$ after delivery of integrated luminosities of 10 fb^{-1} (stars), 100 fb^{-1} (open circles) and 1000 fb^{-1} (filled circles) for $M_{\rm est}$ variable (3). Precisions for mSUGRA points are plotted in Fig. 3(a), constrained MSSM points in Fig. 3(b) and GMSB points in Fig. 3(c). No data are shown for GMSB points for 10 fb^{-1} integrated luminosity due to the poor statistical significance of signal events in this scenario. Note the differing scale in Fig. 3(c) due to the larger spread in $\overline{M_{\rm est}}$ values generated for GMSB models.

Figure 4: The total SUSY particle production cross section $\sigma_{\rm susy}$ plotted against the fitted normalisation of the signal distribution for variable (3) (defined in the text) for 100 random mSUGRA (Fig. 4(a)), constrained MSSM (Fig. 4(b)) and GMSB (Fig. 4(c)) models. In Fig. 4(c) those GMSB models where the gaussian fit to the signal $M_{\rm est}$ distribution failed due to insufficient acceptance are omitted.

Figure 5: Overall non-gaussian precision for measurement of $\sigma_{\rm susy}$ after delivery of integrated luminosities of 10 fb^{-1} (stars), 100 fb^{-1} (open circles) and 1000 fb^{-1} (filled circles) for $M_{\rm est}$ variable (3). Precisions for mSUGRA points are plotted in Fig. 5(a), constrained MSSM points in Fig. 5(b) and GMSB points in Fig. 5(c). No data are shown for GMSB points for 10 fb^{-1} integrated luminosity due to the poor statistical significance of signal events in this scenario. Note the differing scale in Fig. 5(c) due to the larger spread in $\overline{M_{\rm est}}$ values generated for GMSB models.

Model	Variable	$\bar{x}$	σ	$\sigma/\bar{x}$	rms error ($\bar{x}$)	Precision (%)
mSUGRA	1	1.585	0.049	0.031	0.011	2.9±0.3
	2	0.991	0.039	0.039	0.010	3.8±0.5
	3	1.700	0.043	0.026	0.015	2.1±0.3
	4	1.089	0.030	0.028	0.011	2.5±0.3
	5	1.168	0.029	0.025	0.013	2.1±0.2
MSSM	1	1.657	0.386	0.233	0.031	23.1±4.3
	2	0.998	0.214	0.215	0.042	21.1±3.9
	3	1.722	0.227	0.132	0.031	12.8±2.4
	4	1.092	0.143	0.131	0.029	12.8±1.9
	5	1.156	0.176	0.152	0.034	14.8±1.9
GMSB	1	1.660	0.149	0.090	0.037	8.1±1.2
	2	1.095	0.085	0.077	0.040	6.6±1.3
	3	1.832	0.176	0.096	0.034	9.0±1.2
	4	1.235	0.091	0.074	0.041	6.1±1.0
	5	1.273	0.109	0.086	0.034	7.9±2.5

Table 1:

Model	Variable	$\bar{x}$	σ	$\sigma/\bar{x}$	rms error ($\bar{x}$)	Precision (%)
mSUGRA	3	0.855	0.008	0.009	0.003	0.8±0.2
MSSM	3	0.848	0.023	0.027	0.004	2.7±0.5
GMSB	3	0.742	0.141	0.190	0.006	19.0±4.2

Table 2:

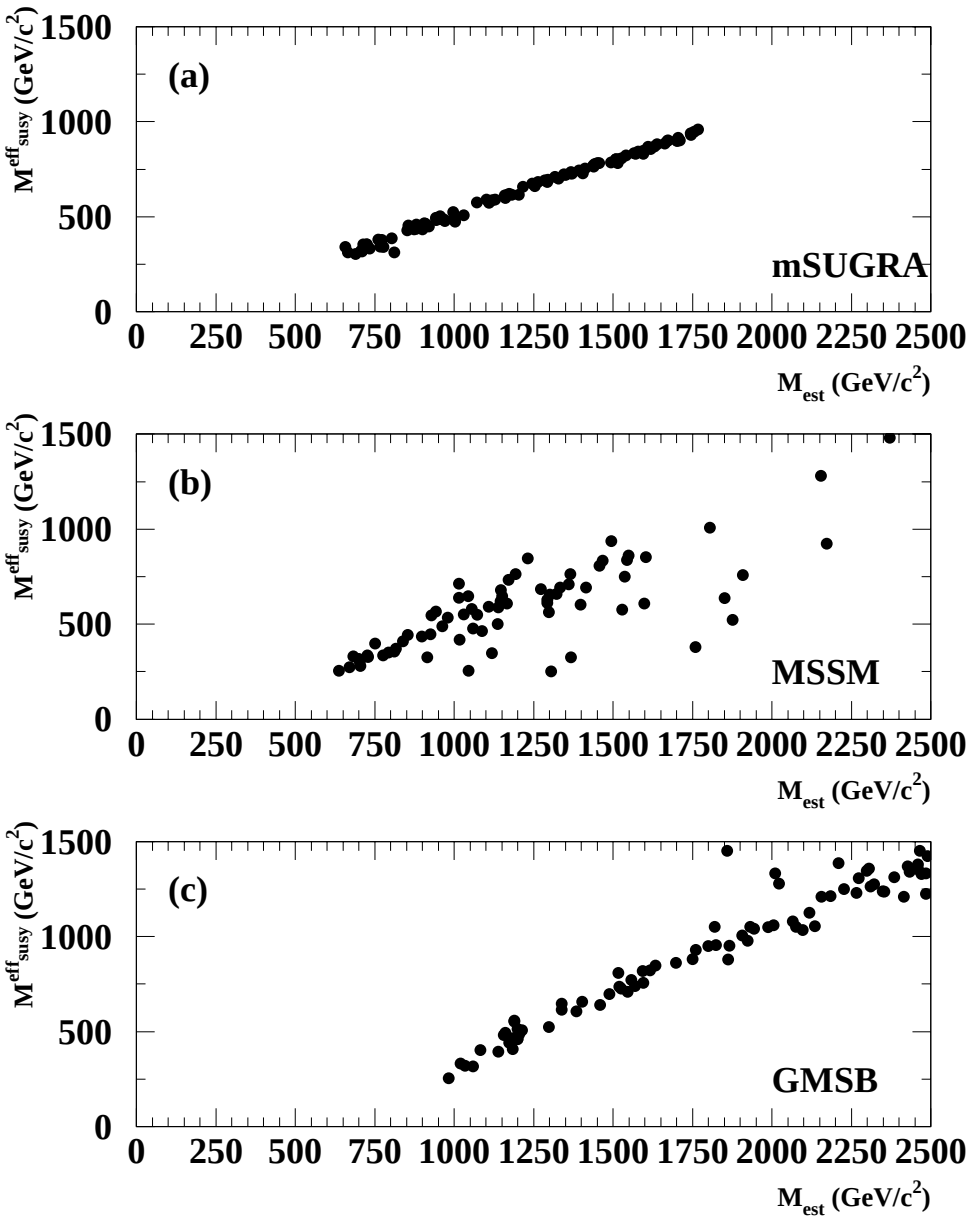
(a)
mSUGRA
(b)
MSSM
(c)
GMSB
M^{eff}_{susy} (GeV/c^2)
M_{est} (GeV/c^2)
0
500
1000
1500
0
250
500
750
1000
1250
1500
1750
2000
2250
2500

Figure 1:

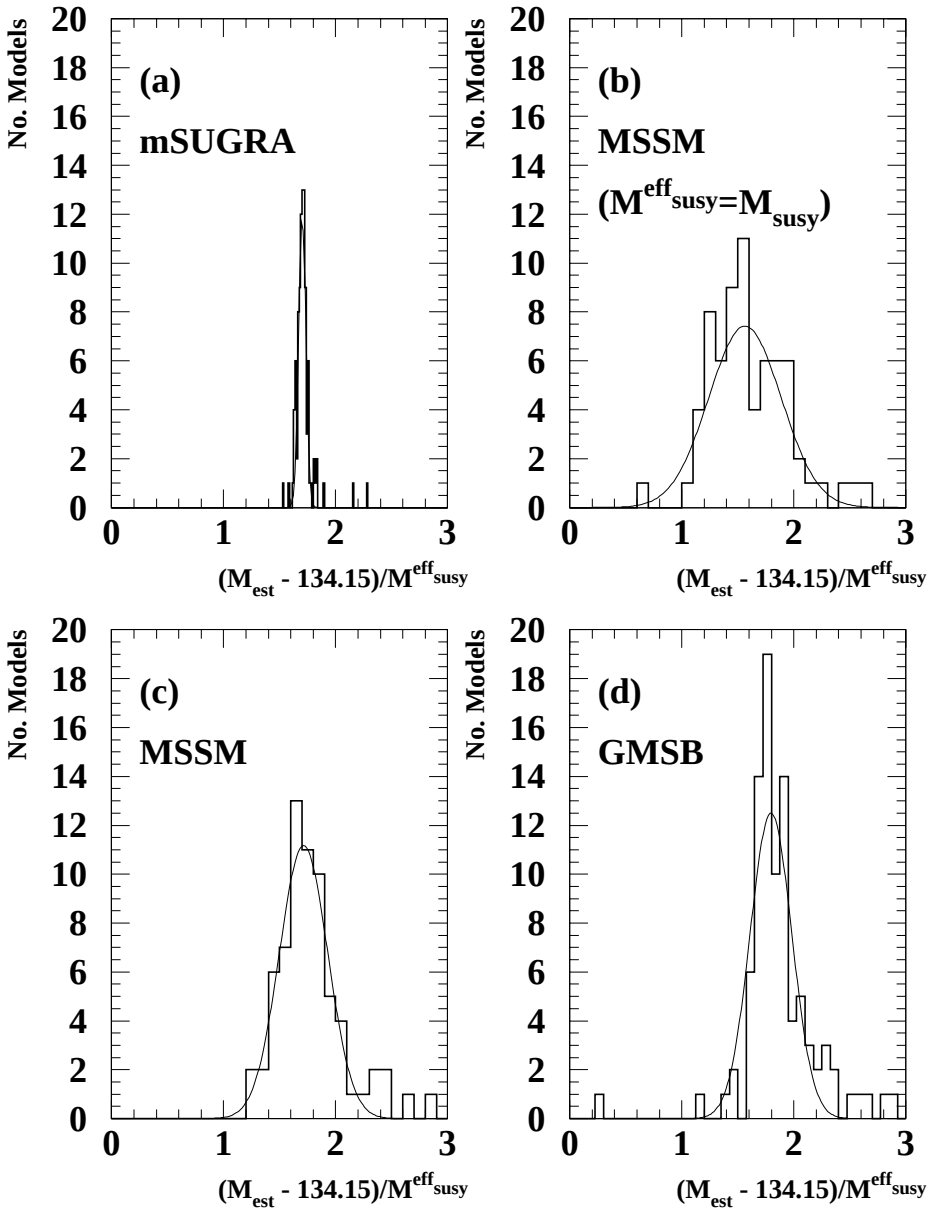
No. Models
(a)
mSUGRA
(b)
MSSM
(M^eff_susy=M_susy)
(c)
MSSM
(d)
GMSB
(M_est - 134.15)/M^eff_susy

Figure 2:

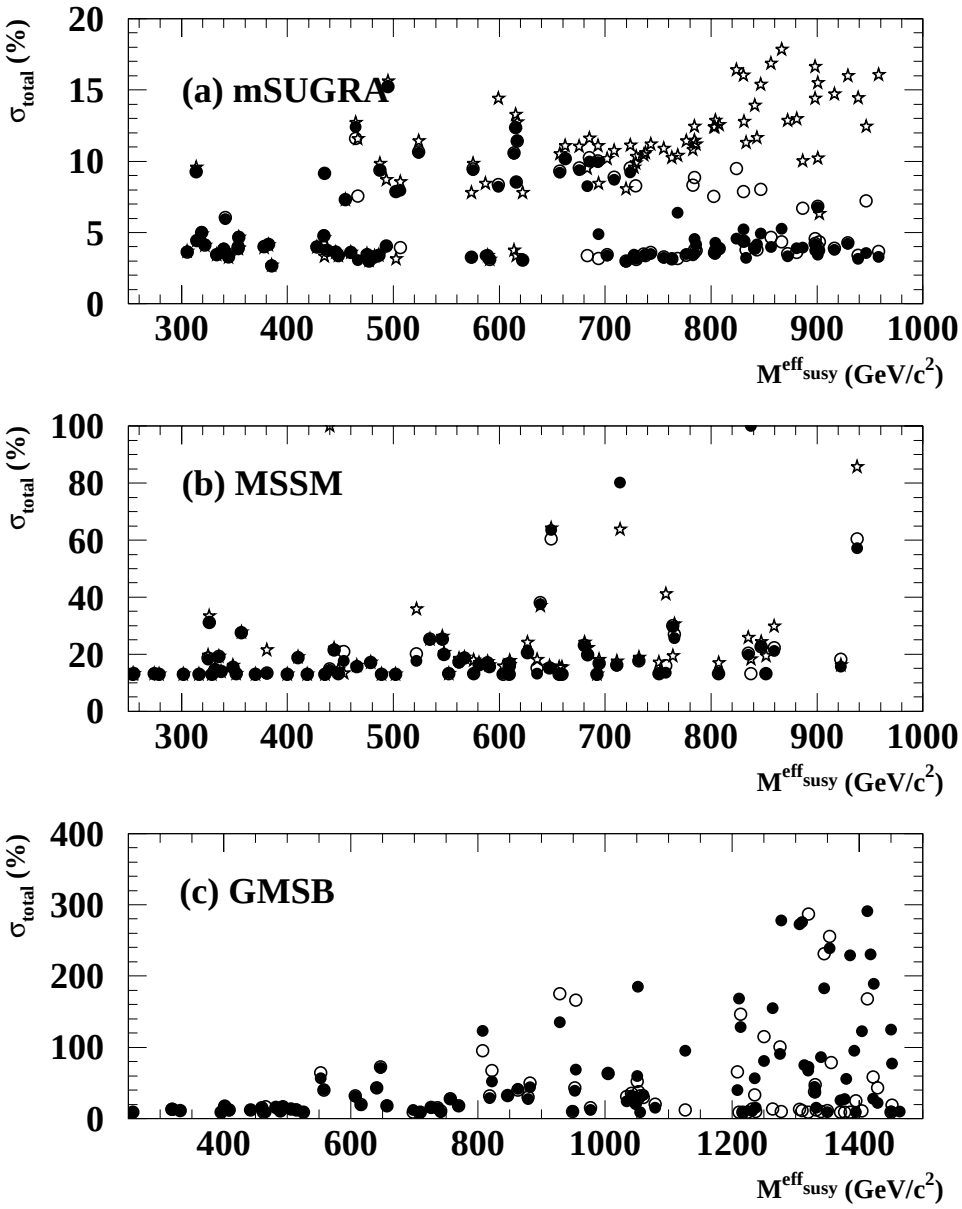

Figure 3:

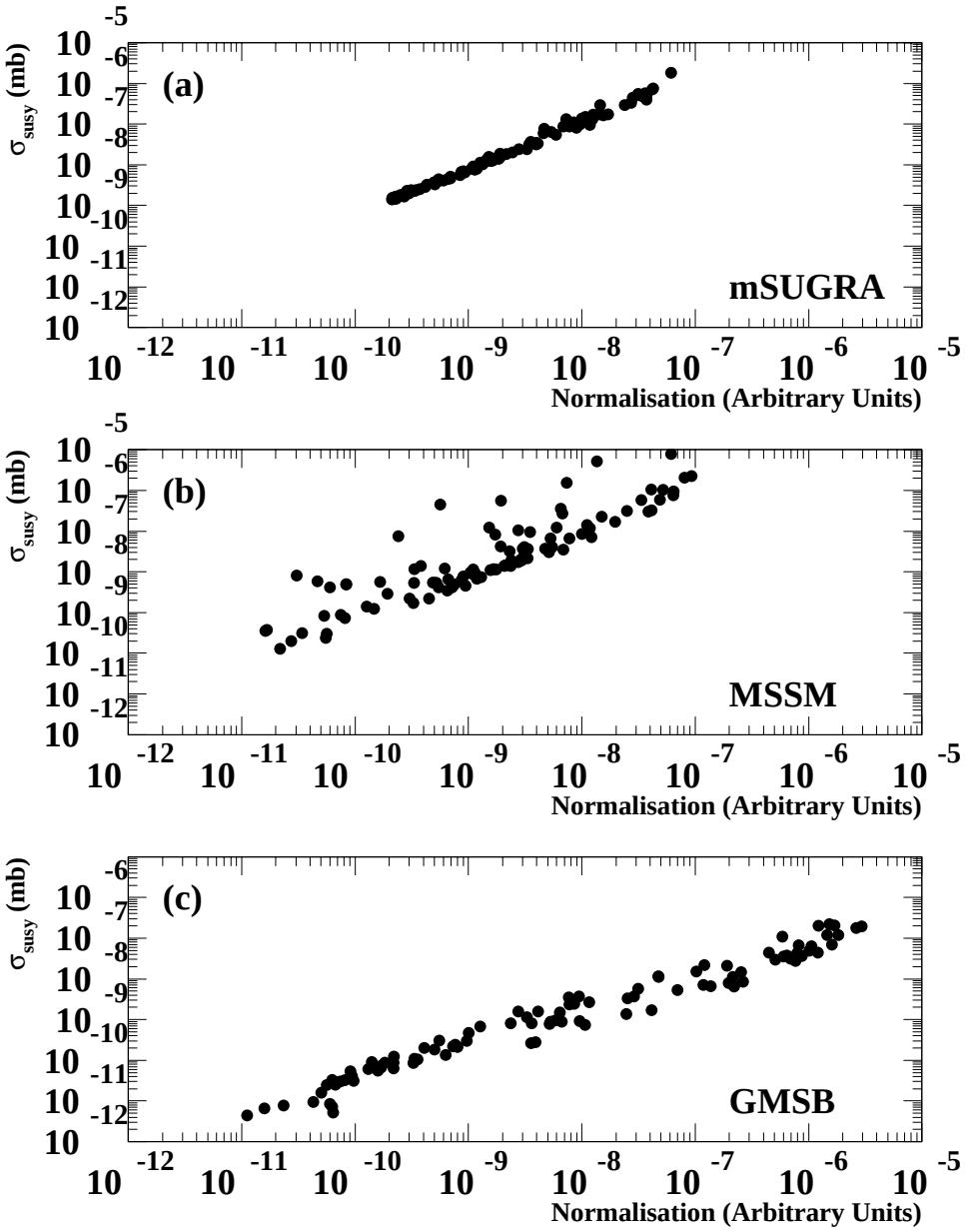
(a)
mSUGRA
(b)
MSSM
(c)
GMSB
σ susy (mb)
Normalisation (Arbitrary Units)

Figure 4:

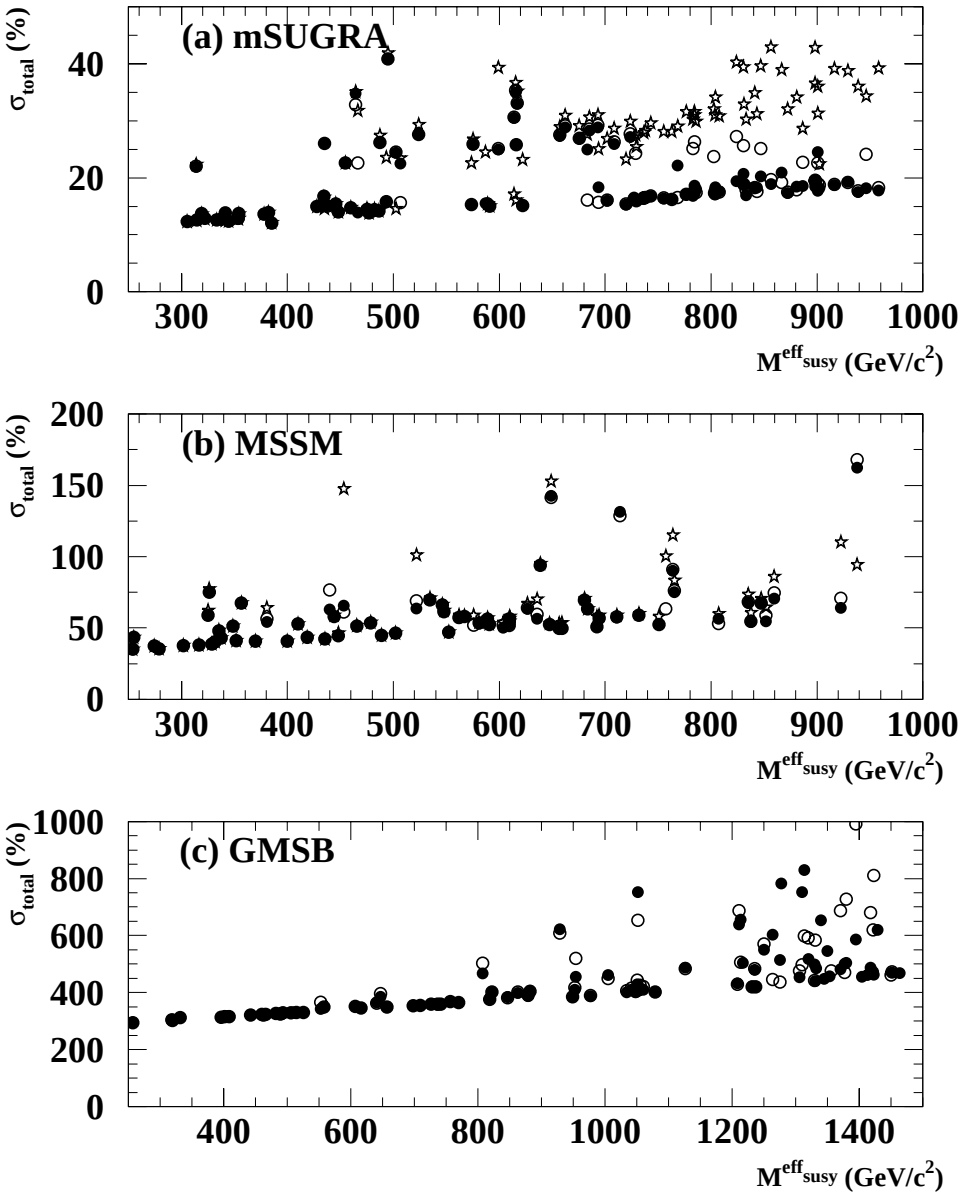
(a) mSUGRA
(b) MSSM
(c) GMSB
σtotal (%)
M^eff_susy (GeV/c^2)
0
20
40
50
100
150
200
200
400
600
800
1000
1200
1400
300
400
500
600
700
800
900
1000

Figure 5: